

Kinetics of the Growth of Anthracene Nanoparticles

Edward Van Keuren,* Elena Georgieva, and Michael Durst

Department of Physics, Georgetown University, Washington,
District of Columbia, USA

ABSTRACT

Nanocrystals of anthracene were formed by “solvent shifting”—reducing the solute solubility by changing the ratio of two components of a binary solvent. Dispersions of slowly-growing nanoparticles with sizes ranging from 100 to 1000 nm were prepared in an acetone/water binary solvent. A model of the growth was developed that described the rapid initial increase in particle size over several minutes, followed by much slower growth over several hours to days. Dynamic light scattering (DLS) measurements of particle size could be described well using this model. UV–VIS and fluorescence spectra suggest that the anthracene particles are crystalline, and exist in equilibrium with molecular anthracene in solution.

Key Words: Nanoparticle; Molecular crystal; Dynamic light scattering; Solvent shifting.

INTRODUCTION

Nucleation is a critical step for many phenomena, including nanoparticle growth^[1] crystallization and biomineralization. A number of techniques for preparing particle dispersions as well as bulk crystals rely on solubility changes to induce nucleation and growth. In one such method, a rapid change in solubility of a particular molecule is induced, often by a solvent exchange from a good to a poorer solvent.^[2–5] A dilute solution of the molecule is rapidly injected into a solvent in which the material has poor solubility but that is miscible with the original solvent. This causes rapid nucleation followed by slower growth as the clusters

aggregate. This method has been applied to prepare dispersions of organic materials in polar solvents, for example, in pharmaceuticals where aqueous formulations are needed for biocompatibility.^[2] It is also valuable for processing materials that cannot be easily formed into large sized bulk crystals, such as the nonlinear optical material polydiacetylene.^[5] In this case, nanoparticles embedded in a polymer matrix yield good optical quality materials.

In a related method, nanoparticles may also be formed in aqueous ternary systems by a “watering out” process, in which supersaturation is induced by decreasing a molecules’ solubility in a binary solvent.^[6] This decrease comes from gradually mixing in more of the

*Correspondence: Edward Van Keuren, Department of Physics, 37th and O Streets, NW, Georgetown University, Washington, DC 20057, USA; E-mail: vankeu@physics.georgetown.edu.



poorer solvent in the binary mixture. Under slow mixing conditions, nanocrystals nucleate and grow.^[7] Both of these "solvent shifting" methods are valuable techniques for preparing and studying organic nanoparticle dispersions,^[8,9] in particular because of the ability to form dispersions at room temperatures.

One question regarding these methods is how the molecules aggregate and grow—whether this is an ordered self-assembly or a random agglomeration of molecules, which rearrange on a slower time scale to form crystals. Here we report an investigation of anthracene nanoparticles formed in an acetone/water solvent. We use dynamic light scattering (DLS) for characterizing particles above ~ 10 nm, and UV–VIS absorption spectroscopy to look at molecular arrangement. These measurements are performed both as functions of composition (ratio of water/acetone in the binary solvent) and as functions of time after changing the solubility. By correlating these results, we can gain insight on the size and structure of the nanoparticles as functions of time and conditions during nucleation and growth.

EXPERIMENT

Sample Preparation

The ternary mixtures are formulated by first preparing a solution of the anthracene (Sigma, 99%) in acetone (Fisher Scientific, spectral grade). Distilled deionized water was rapidly added to this mixture and the sample agitated for several seconds before measurements were started. We have found that the purity of the constituents had little qualitative effect on the overall results; only changes in the mean particle sizes or exact location of the onset of turbidity. We found points in the ternary phase diagram at which particles formed by observing the onset of turbidity as a function of added water.

A series of four compositions with increasing fraction of water were studied in detail. The compositions are listed in Table 1.

Optical Characterization

Dynamic light scattering was used to measure particle diffusion coefficients. Measurements began approximately 30 seconds after agitation ended, since residual fluid motion alters the results severely. Light from an Ar ion laser ($\lambda = 514$ nm) was coupled through a multimode optical fiber into the 1 cm \times 1 cm cross section cuvette. Light scattered at 90° to the incident beam passed through a 50 μ m pinhole to improve the spatial coherence and an interference filter to remove fluorescence and background light, and coupled to a multimode optical fiber. This fiber was coupled to a photon counting avalanche photodiode (EG&G), whose signal was processed by an ALV5000 (ALV GmbH, Germany) hardware autocorrelator. The autocorrelation functions (ACFs) of the scattered irradiance were analyzed using the ALV NonLin routine,^[10] a nonlinear constrained regularization of the autocorrelation function, between delay times of 2 μ s and about 2 ms, and distributions of the scatterer diffusion coefficients were found. In order to determine the corresponding hydrodynamic radii, the Stokes–Einstein equation was used,^[11] along with published values of the viscosity of an water/acetone solvent mixture,^[12] and the ambient temperature (25°C). Since the nanoparticles are likely not spherical, the values of radii presented below should be understood to be effective values demonstrating trends in the particle growth, rather than as an absolute characterization of particle size.

In addition to DLS, UV–VIS (ultraviolet–visible) absorption and fluorescence spectra were measured in order to determine the extent of crystallization. Absorption spectra were measured with a mini-spectrometer from Ocean Optics (Chem 2000) operating between 190 and 890 nm, and a 25 μ m slit width giving a resolution of 1.5 nm. Fluorescence imaging and spectroscopy was performed using a FALCONTM chemical imaging system. The aggregated particles in suspension in a 1 mm cuvette were excited with UV radiation from a mercury lamp, and imaged through a liquid crystal tunable filter with a spectral linewidth of 8 nm.

Table 1. Sample concentrations.

Sample	Mole fraction water	Mole fraction acetone	Mole fraction anthracene
S1	0.0931	0.904	2.80×10^{-3}
S2	0.257	0.742	1.53×10^{-3}
S3	0.504	0.494	5.12×10^{-4}
S4	0.687	0.312	1.29×10^{-4}

RESULTS AND DISCUSSION

Several measurements were taken on undersaturated mixtures (as measured by turbidity). In these, the amount of added water was varied in the samples. In all cases, no particles could be observed in the DLS measurements: the scattered irradiance was about the same as that of a blank (acetone only) cell, and the ACF decayed immediately to zero. From the sensitivity of the instrument, this gives us an upper limit for the cluster sizes in the mixture at about 10 nm.

Particle formation was observed only above a critical water content. The kinetics of the particle growth for the four samples described in Table 1 are shown in Fig. 1. Near this critical water content at which particle formation began, the kinetics of the particle growth were similar to that in naphthalene nanocrystals,^[7] namely, a rapid increase in the first minutes and then a slower growth over a period of hours to days. As seen in the figure, there did not seem to be a clear trend in the time dependences or the particles sizes at which the plateau occurred as a function of the water content. The exact degree of supersaturation was likely different among the samples, which may explain the results. The dispersions were stable over a period of a few hours to days; eventually the particles precipitated.

Phase transitions in multicomponent systems like these are fundamentally different than those in single component systems in the sense that the additional degrees of freedom allow the system to reequilibrate in separate phases. In melt crystallization, for example, the external control of the temperature allows a specific level of supersaturation to be maintained. At this fixed temperature, the material will completely solidify. In solution crystallization, once a sufficient amount of crystals nucleate in a supersaturated solution, the solution

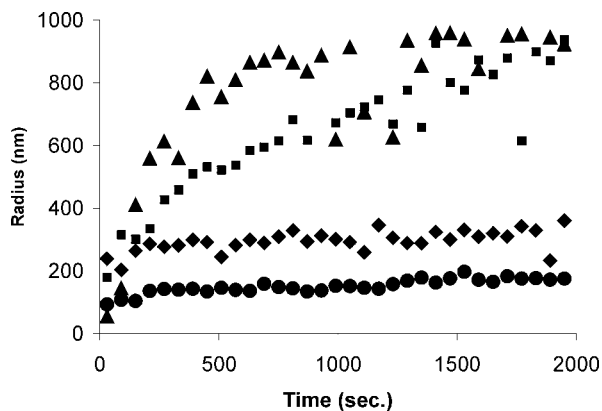


Figure 1. Particle size from DLS measurements vs. time after mixing: S1 = ▲; S2 = ◆; S3 = ■; S4 = ●.

concentration is reduced and further growth will only occur through aggregation of the nucleated particles. In other words, once the solute has repartitioned itself between two phases, the supersaturation condition is removed. Additional solute must be added, solvent removed, or the temperature reduced further in order to maintain supersaturation and crystal growth.

This underlies one significant difference in the nucleation and growth in these systems compared to that in most solution crystallization processes. In the nanoparticles formed in our systems, the supersaturation condition is created initially and the system then allowed to equilibrate. The growth of the particles is accompanied by the depletion of solute from the bulk solution, leading eventually to the end of the supersaturated condition. This process also occurs in the rapid solvent shifting by injection described earlier,^[2-5] but on a much faster time scale.

In order to understand the growth of the particles, we use a simple model describing the mass transport to the particle surface through diffusion, coupled to the decrease in bulk solute concentration. We assume that the growth of the particles is a diffusion-limited process, i.e., once a solute molecule diffuses to the surface of the growing particle, it sticks. Particles are assumed to be spherical, although as noted later, the growth rates determined from the model can be generalized to nonspherical particles. The solute concentration is taken to be initially supersaturated in the bulk, decreasing to a value near the saturation concentration at the particle surface.

The diffusion equation in spherical coordinates

$$J_r \hat{r} = \vec{J} = -D \vec{\nabla} \Phi = -D \frac{\partial \Phi}{\partial r} \hat{r} \tag{1}$$

along with the boundary conditions for the mass concentration Φ : $\Phi(r=a) = \Phi_0$ and $\Phi(r=\infty) = \Phi_1$, where a is the particle radius and D the diffusion coefficient, gives a simple form for the concentration

$$\Phi(r) = \Phi_1 - (\Phi_1 - \Phi_0) \frac{a}{r} \tag{2}$$

and flux at position r

$$J_r(r) = -D(\Phi_1 - \Phi_0) \frac{a}{r^2} \tag{3}$$

From this equation, we find the rate of mass accumulation inside a sphere surrounding the particle to be

$$\frac{dm}{dt} = 4\pi D(\Phi_1 - \Phi_0)a \tag{4}$$



which then gives a rate of change of the radius

$$\frac{da}{dt} = \frac{D(\Phi_1 - \Phi_0)}{\rho a} \quad (5)$$

for solute density ρ . For constant values of the boundary conditions (concentrations), the particle radius will increase continuously with a $t^{1/2}$ dependence. However, in our system the boundary condition at $r = \infty$ (bulk solution concentration) will change over time as the particles grow. Specifically, the supersaturated solute in the bulk will be depleted, leading to a leveling off of the particle radius at longer times. This is incorporated in the model by adding a dependence of the bulk concentration on the particle radius. The bulk concentration is now

$$\Phi_1 = \Phi_{10} - \frac{4\pi\rho N}{3} [a^3(t) - a_0^3] \quad (6)$$

where Φ_{10} is the initial bulk concentration, ρ is the solute density, N is the number of particles per unit volume initially present, and a_0 is the initial particle radius. Substituting this into the differential Eq. (5) and integrating gives a complicated form for the dependence of the radius a on time:

$$t = \frac{3}{4\pi ND} \left[\frac{1}{6C} \ln \left(\frac{C^3 + x^3}{(C+x)^3} \right) + \frac{1}{\sqrt{3}C} \tan^{-1} \left(\frac{2x-C}{\sqrt{3}C} \right) \right]_{a_0}^a \quad (7)$$

with the constant

$$C = \left[\frac{3}{4\pi\rho N} (\Phi_0 - \Phi_{10}) - a_0^3 \right]^{1/3}$$

The variable x is evaluated between the limits a_0 and a .

While Eq. (7) cannot be explicitly solved for the radius as a function of time, the data can be fit numerically to find the values of the parameters. We used fixed values of the parameters $\rho = 1.24 \text{ g cm}^{-3}$, and $a_0 = 10 \text{ nm}$, Φ_{10} is calculated for the particular mixture, and let the parameters N (number density of nucleation sites) and $\Delta\Phi_0$ [$= (\Phi_{10} - \Phi_0)/\Phi_0$, initial relative supersaturation] vary in the fit. The density is the literature value for anthracene, and the initial particle radius is taken as the lower limit of resolution of the measurements; its exact value had little effect on the final fit. The diffusion coefficients used for S1 and S3 ($D = 1.8 \times 10^{-5}$, $1.0 \times 10^{-5} \text{ cm}^2 \text{ s}^{-1}$, respectively) are obtained by correcting the literature value in water^[13] ($D = 7.74 \times 10^{-6} \text{ cm}^2 \text{ s}^{-1}$) for the viscosities of the binary solvent.^[12] The results are shown in Figs. 2 and 3 for two of the samples in which a clear particle growth could be observed. For the other two mixtures depicted in Fig. 1, the particles reached the plateau in growth quickly, and so little information could be found from the fit results. The relative supersaturation [$= (\Phi_1 - \Phi_0)/\Phi_0$] found using Eq. 6, is also plotted.

Good fits to the data sets could be obtained. The values obtained from the fit are given in the figure captions for the two plots. While the complexity of Eq. (7) hides the physics underlying the kinetics, we

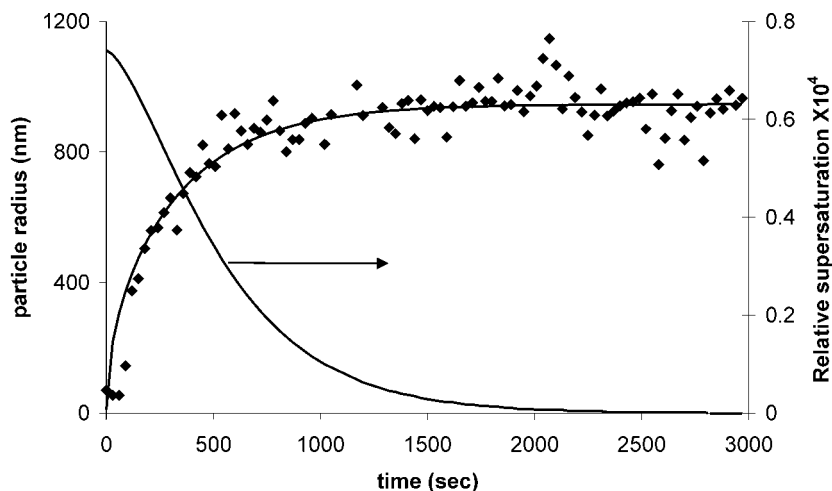


Figure 2. Dynamic light scattering data from S1 along with a fit using Eq (7). The calculated relative supersaturation vs. time is also shown. $N = 1.2 \times 10^5 \text{ cm}^{-3}$, initial supersaturation ratio = 7.3×10^{-4} .

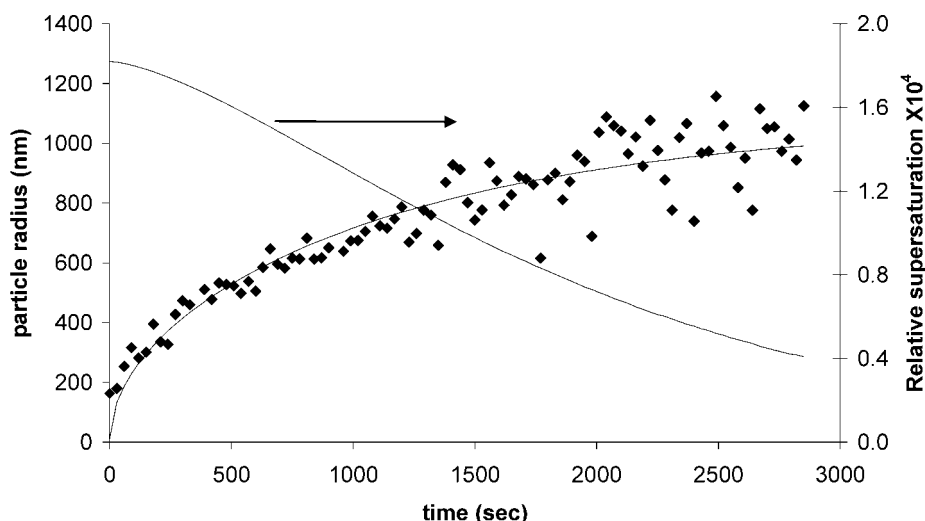


Figure 3. Dynamic light scattering data and calculated relative supersaturation from S3 along with a fit using Eq. (7). $N = 5.6 \times 10^4 \text{ cm}^{-3}$, initial supersaturation ratio = 1.8×10^{-4} .

can set the bulk concentration (Φ_1) equal to the final value Φ_0 in Eq. (6) to find the maximum radius:

$$r_{\max} = \left[\frac{3}{4\pi\rho N} (\Phi_{10} - \Phi_0) + a_0^3 \right]^{1/3} \quad (8)$$

From this we see that the ratio of $\Delta\Phi_0$ to the number density of nucleation centers, N , is fixed by the long time particle radius. This ratio also occurs in the constant C in Eq. (7), which is also the only place the concentration difference appears. The number density of nucleation centers also appears as a scaling factor for t in Eq. (7). In summary, the value of the maximum radius sets the ratio of the fit parameters, and the parameter N is further fixed by the initial growth rate.

A number of approximations were assumed in deriving this behavior of the particle growth. The concentration at the growing particle surface has been assumed to be a constant value close to the saturation concentration. The physical reasoning behind this is that the average solute molecule near a nucleated surface will join the crystal if the total change in Gibbs free energy is negative, so the equilibrium concentration there will be close to saturation. However, we neglect the surface term in the free energy difference, which will mean the equilibrium concentration at the surface will have a dependence on the particle size. This can lead to Ostwald ripening, an effect in which larger particles grow while smaller ones dissolve.^[6]

We also implicitly assume that we start with nucleation sites that are already larger than the critical size, that the distribution is monodisperse, that the growth rates are

identical and that the particles grow independent of each other, connected only through the dependence on the bulk concentration. The most prominent assumption, that we have spherical particles, is clearly untrue at both short (small number of molecules per particle) and long (precipitated crystals) times. However, the model is still valid if we consider length scales larger than the particle sizes. The radius in this case is an effective radius corresponding to a spherical particle with the same volume increase. The exact correspondence between this effective radius and the radius determined from DLS is unknown, so while the data can be fit well, the results should not be strictly interpreted quantitatively.

The basic idea of the model, that the growth of monodisperse systems proceeds from an assembly of identical primary particles formed in a rapid burst of nucleation, followed by growth, by addition of monomers diffusing to the particle surface, was already described by LaMer in 1950.^[14] In the current understanding, this simple model is valid only during the initial growth stages.^[15] Many theoretical and computational models have been developed to more accurately describe the growth of particles.^[16] Whereas most of these are geared towards crystallization processes in which there is a continual monomer feed, the main advantage of the simple model we use here is that it accounts for the depletion of the monomer in the bulk in the formation of our particles.

The value of the diffusion coefficient used in the fitting procedure has a strong effect on the values of the fit parameters. The initial growth rate is set by both the speed of diffusion of molecules to the particle surface



and the average distance they travel, which depends on the number of nucleation centers. The value used for D is certainly too high; a number of studies have shown drastic decreases in the diffusion coefficient at and above saturation, attributed to the formation of clusters.^[17] For a given fit, the calculated number of particles will scale inversely with the diffusion coefficient used, so the actual number density of particles is probably much higher than given ($N = 1.2 \times 10^5 \text{ cm}^{-3}$ and $N = 5.6 \times 10^4 \text{ cm}^{-3}$ for S1 and S3 respectively). Likewise, the relative saturation will scale inversely with particle number density, resulting in larger ratios than noted above. In addition, the model oversimplifies the diffusion process by a constant value of D ; in fact it will change considerably as the supersaturation is reduced. These differences may explain the low value of the relative supersaturation compared to most crystallizing systems.^[6]

The functionality of the model does describe the results in terms of the initial growth of primary particles through diffusion of molecules to the surface, with a leveling off of particle size vs. time due to the depletion of solute. Subsequent particle growth is likely due to aggregation of the primary particles over a period of several days. It is also consistent with qualitative long time observations from mixtures with water content just below the onset of turbidity. As described earlier, no consistent measurements of particle formation were observed in these, however, experimental measurements of the scattered irradiance typically contained sporadic peaks corresponding to large particles present in the mixtures. These appeared only near the critical saturation points, not in mixtures well below the transition point

(onset of turbidity). In the model, these are mixtures above saturation in which a small number of particles form and deplete the solute.

In real samples, a number of other effects need to be considered.^[18] In most crystallization processes, there is strong evidence of heterogeneous nucleation, i.e., the nucleation induced by foreign material or container walls.^[19] We have assumed a distribution of growing particles at the start, but impurities may induce additional nucleation over time. Finally, the binary solvent will likely not be homogeneous at the molecular scale; the water will likely have a different structure near the interfaces,^[20] and there is likely to be an acetone-rich solvent cage around the anthracene, both initially and after they aggregate. It is likely that these effects will have a significant influence affect how the molecules assemble and grow.

Figure 4 shows the absorption spectra from anthracene in acetone only and in the $1.29 \times 10^{-4}/0.312/0.687$ (mole fractions) anthracene/acetone/water mixture (S4) at several times after mixing. The spectrum of anthracene in acetone matches literature values for the anthracene molecular absorption,^[21] with the S1 energy level transition near 380 nm. On dimerization into a T-structure, the absorption bands shift to lower energies, with the lowest vibrational sublevel of the S1 state moving to 402 nm. Larger size aggregates show a shift back to the blue, with the lowest energy transition at 397 nm (all literature values measured at 77K). A nanoparticle dispersion of anthracene prepared with the rapid nucleation method described earlier^[3] shows this shift due to dimerization/crystallization clearly. This dispersion scattered strongly,

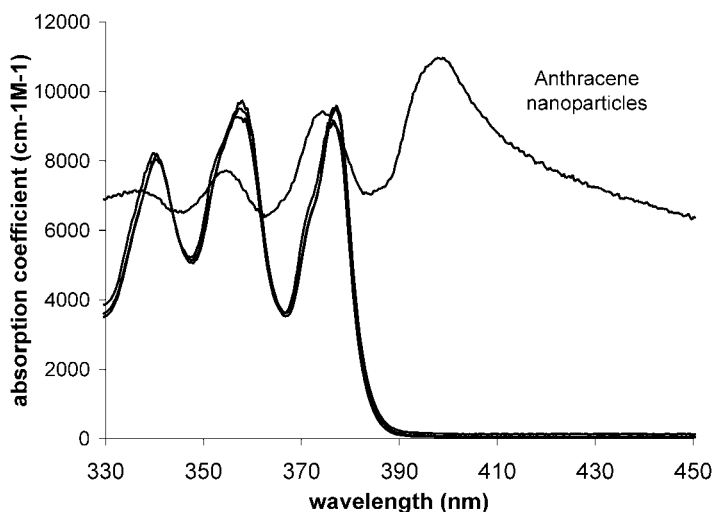


Figure 4. Absorption spectra of anthracene in pure acetone and in the binary solvent (sample S4) at two times after mixing (2 min, 32 min). The curve labeled anthracene nanoparticles is from a dispersion prepared using rapid nucleation. The spectra of anthracene in pure acetone and in the binary solvent are indistinguishable.

giving a featureless background, but the peaks are still clearly visible.

Despite the increase in particle size measured by DLS, no changes are seen in the absorption spectra of the ternary mixtures. In all cases, there are only insignificant shifts in the observed peaks from the pure anthracene solution. The likely explanation for the lack of change in the absorption is that despite the large turbidity increase in the mixture, most of the anthracene still exists in molecular form. This is corroborated by imaging measurements of the fluorescence emission spectra of the different samples.

Figure 5 shows images taken with a FALCONTM Chemical Imaging Microscope (ChemIcon, Inc., PA) of a sample of anthracene in a binary solvent with high water content. The image on the left is a standard transmission image, while the right image is the fluorescence emission at a wavelength of 450 nm. A mercury UV lamp is used as the excitation source, with a longpass filter cutting the emission below 400 nm. Both images appear to show anthracene crystallites. The fluorescence emission spectrum of the large crystallite near the center of the image is shown in Fig. 6, compared with spectra of an acetone solution of anthracene and from the nanoparticles prepared by the injection method. In this latter sample, all the anthracene is in particulate form, since the final solvent used is almost pure water. Here, the shift in the absorption spectrum with respect to the solution spectrum indicates crystallinity of the anthracene. The location of the emission bands is identical between the nanoparticle samples, which suggests that the particles formed in our

method are also crystalline. The main emission band is shifted to higher wavelengths in the solution spectrum. The direction of the shift is surprising, since published data indicates shifts to lower energies in the dimers and crystals, similar to that in the absorption spectra. However, the data is not clear enough to allow precise identification of the lines—the solution maximum at 455 nm may correspond to the nanoparticle peaks at 478 nm rather than the maxima at 450 nm.

CONCLUSION

Solvent shifting provides an interesting method of preparing and studying nanoparticle dispersions of organic molecules under well-controlled growth conditions. When the solute solubility is reduced to achieve supersaturation, there is a rapid increase in particle growth that levels off within several minutes. An investigation of several points on the ternary phase diagram of the anthracene/acetone/water system did not reveal any systematic dependence of the growth kinetics on the ratio of water to acetone in the solvent. However, we found that the data follow a simple model of diffusion-limited aggregation coupled to a decrease in supersaturation. The results of a two-parameter fit of this model to the data give reasonable results, however, they are only qualitative due mainly to the lack of an accurate value for the diffusion coefficient as a function of supersaturation. In this model, the value of this stabilized particle size is fixed by the ratio of the initial relative supersaturation to the number density of nucleation sites, while the initial

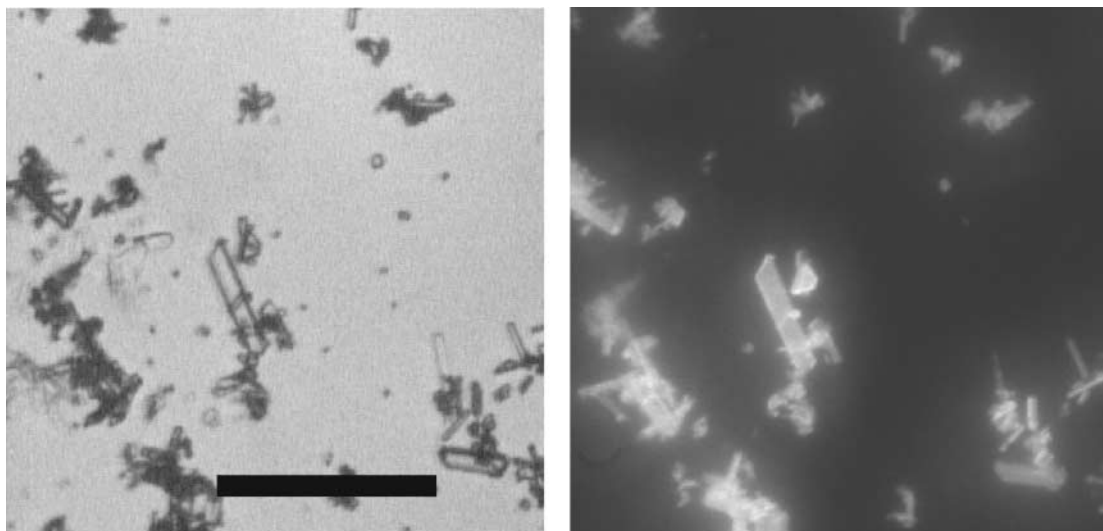


Figure 5. Micrographs of highly aggregated anthracene crystals in binary solution. On the left is the transmission image, on the right is a fluorescence emission at $\lambda = 450$ nm. The bar in the image is 75 μm long.



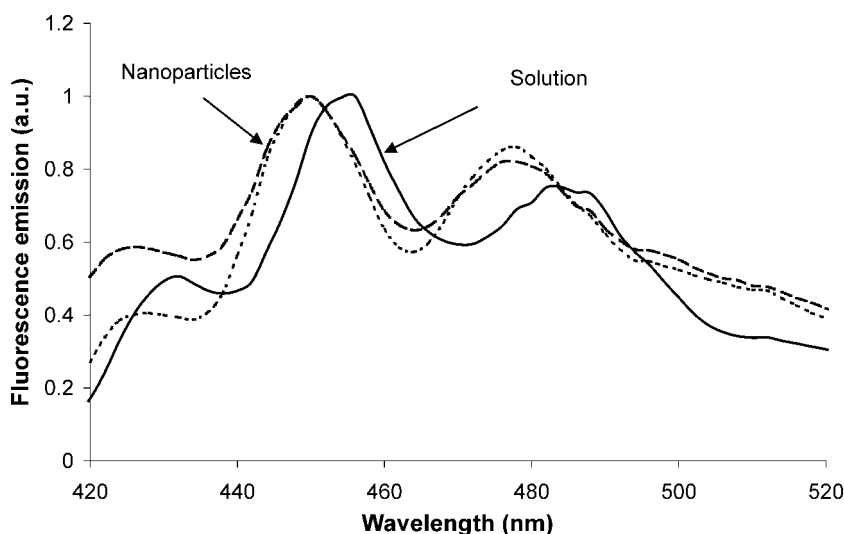


Figure 6. Fluorescence emission from anthracene in solution and anthracene nanoparticles (produced by two different methods).

growth rate is set by the diffusion coefficient and degree of supersaturation.

The mechanism of the nucleation on the molecular scale could not be followed, however, the particles that eventually precipitated out of solution were crystalline, as determined by fluorescence emission and UV-VIS absorption spectroscopy. These spectral changes could only be seen in images of the precipitated particles, not in the ternary mixtures, in which most of the anthracene exists in solution in equilibrium with the nanoparticles.

REFERENCES

- Alivisatos, A.; Barbara, P.; Castleman, A.; Chang, J.; Dixon, D.; Klein, M.; McLendon, G.; Miller, J.; Ratner, M.; Rossky, P.; Stupp, S.; Thompson, M. From molecules to materials: current trends and future directions. *Adv. Mater.* **1998**, *10* (16), 1297–1336; Herron, N.; Thorn, D. Nanoparticles: uses and relationships to molecular cluster compounds. *Adv. Mater.* **1998**, *10* (15), 1173–1184; Whitesides, G.; Mathias, J.; Seto, C. Molecular self-assembly and nanochemistry: a chemical strategy for the synthesis of nanostructures. *Science* **1991**, *254*, 1312–1319.
- Horn, D. Preparation and characterization of microdisperse bioavailable carotenoid hydrosols. *Die Angew. Makromol. Chemie* **1989**, *166/167*, 139–153.
- Kasai, H.; Nalwa, H.; Oikawa, H.; Okada, S.; Matsuda, H.; Minami, N.; Kakuta, A.; Ono, K.; Mukoh, A.; Nakanishi, H. A novel preparation method of organic microcrystals. *Jap. J. Appl. Phys.* **1992**, *31*, L1132–L1134.
- Murray, C.; Norris, D.; Bawendi, M. Synthesis and characterization of nearly monodisperse CdE (E = S, Se, Te) semiconductor nanocrystallites. *J. Am. Chem. Soc.* **1993**, *115*, 8706–8715.
- Matsuda, H.; Yamada, S.; Van Keuren, E.; Katagi, H.; Kasai, H.; Okada, S.; Oikawa, H.; Nakanishi, H.; Smith, E.; Kar, A.; Wherret, B. Nonlinear refractive indices of polydiacetylene microcrystals. *Proc. SPIE* **1997**, *2998*, 241–248.
- Mullin, J.W. *Crystallization*, 4th Ed.; Butterworth-Heinemann: Oxford, UK, 2001.
- Van Keuren, E.; Georgieva, E.; Adrian, J. Kinetics of the formation of organic molecular nanocrystals. *Nano. Lett.* **2001**, *1*, 141–144.
- Horn, D.; Rieger, J. Organic nanoparticles in the aqueous phase – theory, experiment and use. *Angew. Chemie Int. Ed.* **2001**, *40*, 4330–4361.
- Texter, J. Precipitation and condensation of organic particles. *J. Disper. Sci. Tech.* **2001**, *22*, 499–527.
- Peters, R. Noise on photon correlation functions and its effects on data reduction algorithms. In *Dynamic Light Scattering. The Methods and Some Applications*; Brown, W., Ed.; Clarendon Press: Oxford, UK, 1993; 149–176.

11. Atkins, P. *Physical Chemistry*; Oxford Univ. Press: Oxford, UK, 1978; 835.
12. Noda, K.; Ohashi, M.; Ishida, K. Viscosities and densities at 298.15K for mixtures of methanol, acetone and water. *J. Chem. Eng. Data* **1982**, *27* (3), 326–328.
13. <http://www.rrc.state.tx.us/divisions/og/riskguidelines/table4-4physical.pdf>. Accessed on June 10, 2003.
14. LaMer, V.K.; Dinegar, R. Theory, production and mechanism of formation of monodispersed hydro-sols. *J. Amer. Chem. Soc.* **1950**, *72*, 4847–4854.
15. Matijević, E. Uniform inorganic colloid dispersion. Achievements and challenges. *Langmuir* **1994**, *10*, 8–16, and references therein.
16. Schmelzer, J.; Röpke, G.; Mahnke, R. *Aggregation Phenomena in Complex Systems*; Wiley-VCH: Weinheim, 1999.
17. Mohan, R.; Kaytancioglu, O.; Myerson, A. Diffusion and cluster formation in supersaturated solutions of ammonium sulfate at 298 K. *J. Cryst. Growth* **2000**, *217*, 393–403.
18. Dunning, W. General and theoretical introduction. In *Nucleation*; Zettlemoyer, A., Ed.; Marcel Dekker: New York, 1969; Chap. 1, 1–68.
19. Liu, X. A new kinetic model for three-dimensional heterogeneous nucleation. *Langmuir* **2000**, *16*, 7337–7345.
20. Robinson, R.; Stokes, R. Properties of ionizing solvents. In: *Electrolyte Solutions; The Measurement and Interpretation of Conductance, Chemical Potential, and Diffusion in Solutions of Simple Electrolytes*, 2nd Ed.; Butterworths: London, 1965; Chap. 1.
21. Chandross, E.; Ferguson, J.; McRae, E. Absorption and emission spectra of anthracene dimers. *J. Chem. Phys.* **1966**, *45* (10), 3546–3553.

Received June 23, 2002

Accepted January 20, 2003



